Formation MicroScanner Providing Better Answers for Carbonate Secondary Porosity in Alamein Dolomite Formation, NW Desert, Egypt

Mohamed R. Shalaby, Nurhazwana Jumat * and **Md. Aminul Islam**

Department of Physical and Geological Sciences, Universiti Brunei Darussalam, JalanTungku Link, Gadong BE1410, Brunei Darussalam; ragab.shalaby@ubd.edu.bn (M.R.S.); aminul.islam@ubd.edu.bn (M.A.I.)
* Correspondence: nurhazwanajumat@gmail.com; Tel.: +673-8125090

Abstract: The use of borehole imaging tools has become widespread in recent years with more specialized studies of reservoir properties, particularly in highly-porous and fractured carbonate systems. In this study, the Formation MicroScanner (FMS) borehole imaging tool and conventional well log data have been used to study the secondary porosity of the dolomitic Alamein Formation in the Alamein Field, north Western Desert, Egypt. Based on well log analyses of the formation from Tourmaline-1X and N.Alamein-6X wells, we show that secondary porosity occurs across the formation, and is filled mostly with hydrocarbon. We also show that the formation has good average effective porosity and hydrocarbon saturation. FMS images of the Tourmaline-1X well confirms that the formation is intermittently vuggy with solution-filled channels from the top to its base. The vug pores are observed to be well-connected, which supports good effective porosity values interpreted from petrophysical data. An additional set of core photographs of the Alamein Formation from N.Alamein-5X well confirms the presence of secondary pores, which are filled by hydrocarbon, and exhibit intense fluorescence under UV light. Our results show that the abundance of secondary porosity in Alamein Formation would play a key role in evaluating its reservoir quality and reservoir performance.

Keywords: borehole imaging; secondary porosity; formation evaluation; Egypt; vugs; fractures; formation microscanner; north western desert; well logging; petrophysical

1. Introduction

Secondary porosity is an important feature in carbonates. All carbonate reservoir rocks have undergone significant diagenesis, so the understanding of their diagenetic history is important in order to understand their depositional history and the reservoir quality evolution [1].

In carbonate reservoirs, hydrocarbon production strongly depends on fractures and secondary porosity. The different methods and data used for reservoir fracture identifications include: core, image log, wireline log, well test, thermal survey, mud loss and stoneley wires [2]. Core analysis has been the main source for obtaining data from small-scale fractures observed in boreholes. However, availability of such data is often limited by the cost and availaibility of core samples. Conventional subsurface one-dimensional wireline logging techniques have been previously used to evaluate clastic and carbonate reservoirs in many study areas [3–9]. However, these tools should be applied considering the limitations defined by formation heterogeneity and the tool resolution [8]. In the past, defining many depositional and diagenetic facies was complicated by decimeter-scale resolution range for many of the previously used logging tools [10]. Application of 2D borehole imaging overcomes many of these limitations and enables imaging of lateral variations of the rock properties, including detection of the

secondary porosity structures such as vugs, fractures and channels .The use of borehole imagery has become more widespread in recent times, particularly utilized to study the factors controlling porosity and permeability [11–15]. However, borehole images only produce information in the borehole and other important information such as hydrocarbon content of the true formation cannot be obtained from them. Hence, borehole imaging tools do not replace the conventional logging data and should be used considering the associated limitations. The best results are obtained when both imaging and traditional one-dimensional logging techniques are used together, complimenting each other.

Borehole imaging tools produce an image of the borehole wall typically based on physical property contrasts. The two principal imaging devices utilized in the industry are electrical and ultrasonic borehole imaging tools. An ultrasonic device is based on acoustic reflectivity from the borehole wall, and record amplitude and travel time. Examples include the borehole televiewer (BHTV), circumferential borehole imaging tool (CBIL) and ultrasonic borehole imager (UBI). Electrical imaging is based on conductivity and resolves finer scale features. Dark areas on the image indicate low resistivity, whereas light indicates areas of high resistivity. Some examples are formation microimager (FMI), formation microscanner (FMS) and electrical microimaging (EMI). In this paper, an electrical FMS imaging tool is used to study secondary porosity in Alamein Formation. Notable features observed on image tools include vugs and fractures. Vugs are pore spaces inside rocks that are typically formed by any of the following: cracks and fissures opened by tectonic activity, open spaces within ancient collapse breccias, dissolution or erosion of mineral crystals or fossils inside a rock matrix. Vuggy porosity is divided into two groups according to how the pore space is connected: 'Separate vugs' (such as ooids or skeletal material, and intrafossil porosity) and 'touching vugs'. The isolation of separate vugs adversely affects the permeability. Drilling-induced fractures (DIFs), on the other hand, are typically created when stresses around a borehole exceed that required to cause tensile failure of the wellbore wall [15]. Evaluation of secondary porosity and fractures in relation to hydrocarbon conduits has been covered by many [16–21].

In this study, FMS is utilized to evaluate the reservoir quality and secondary porosities, resulting from diagenetic processes, of the dolomitic Alamein Formation in the Alamein Field. Petrophysical and well log and core data from the formation are also utilized to produce an integrated study of secondary porosity evaluation of the Alamein Formation.

2. Study Area

2.1. Lithostratigraphy

The Western Desert covers two-thirds of the whole area of Egypt. The coastal basins of Matruh, Shushan, Alamein and Natrun are located in the northern half of the Western Desert. The area of study covers the Alamein Field (Figure 1), located between latitudes $28°00'$–$30°00'$ S and longitudes $28°00'$–$30°00'$ E. The lithostratigraphic column in the northern part of the Western Desert comprises formation intervals from Pre-Cambrian basement rocks to recent deposits. The thickness of the sedimentary section is about 14,000 feet. Throughout the entire Mesozoic and a large part of the Cenozoic period, the northern Western Desert existed as a broad shelfal area at the southern margin of the neo-Tethys Ocean and experienced multiple transgression-regression cycles, which resulted in the formation of alternate carbonate and clastic deposits [22].
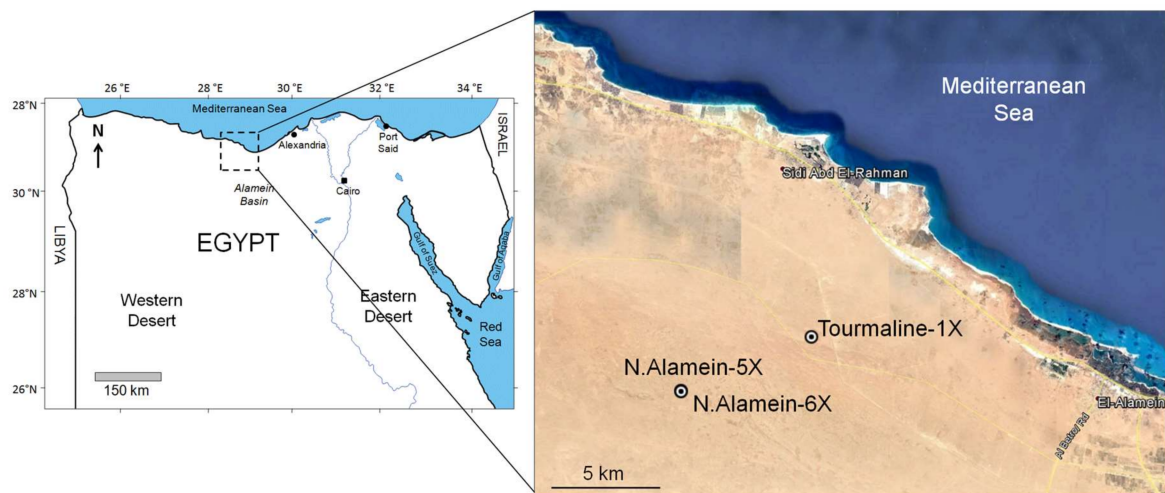
Figure 1. Location of the project wells within Alamein Field, Western Desert, Egypt.

2.2. Hydrocarbon Potential

The tectono-stratigraphic history of the Western Desert resulted in the creation of the various reservoir and seal combinations and contributed to formation of oil deposits. Consequently, high potential reservoirs are widespread in the area [23,24]. Most of these reservoirs are related to structures that were initiated during the Late Cretaceous-Eocene period and are located within or at the edges of the early depocentres. These structures eventually became kitchen areas for hydrocarbons [25].

Hydrocarbons in the Western Desert are present in sediments of various stratigraphic periods, including the Paleozoic, Mesozoic (Jurassic and Cretaceous) and Tertiary (Eocene), with the most prolific oilfields mostly restricted to the Cretaceous sediments. According to Metwalli and Abd El-Hady [26], oil and gas pay zones in the Western Desert include, from top to base, Lower Miocene sandstone, Turonian carbonate rocks, Cenomanian carbonate rocks, Cenomanian clastic rocks, Aptian dolomite, Aptianclastic rocks and Middle Jurassic sandstone. The carbonate reservoirs of the Western Desert consist of dolomites and limestones from the Cretaceous age [27,28]. Sandstone reservoirs include the Jurassic Khatatba and Ras Qattara Formations from the Jurassic age, Alam El-Bueib and Kharita Formations of Lower Cretaceous age, Bahariya Formation and Abu Roash "C" and "E" members from the Upper Cretaceous age (Figure 2). Hydrocarbon production in the northern part of the Western Desert, which was used for the present study, is concentrated exclusively in the Aptian and the Cenomanian-Turonian carbonate-clastic reservoirs.

In the northern Western Desert, the most important carbonate reservoir is the Aptian Alamein Dolomite [22]. The Alamein Dolomite, which is the focus of this study, is one of the most prolific oil producing reservoirs and the first commercial reservoir discovered in the Western Desert. The Alamein Field was discovered in 1966 and commenced production in 1968. It is part of the Alamein-Yidma block which also comprises of Zain and Yidma fields. In 2012, it was reported that the fields are estimated to contain initial recoverable oil reserves of 12.1 million barrels (MMbbl), of which 7 MMbbl remain [29]. The Alamein Field is one of the largest fields discovered to date in the area.

The Alamein Formation consists of fractured microcrystalline dolomites with minor shales of Lower Cretaceous Mid-Aptian age. It is a shallow marine carbonate layer and it represents a fine-grained break, between the two sandstone cycles of Kharita Formation at the top, and the underlying Alam El-Buib Formation. Based on the petrographic study done by Zein El-Din et al. [24], the Alamein Formation has undergone dolomitization and contains variable amounts of calcite with anhydrite and iron oxide as minor minerals. Badr and Ayoub [30], after analysis of microelectrical borehole images, concluded that many of the Middle Eastern carbonate reservoirs, in spite of their reputation for being homogeneous deposits, are very heterogeneous.
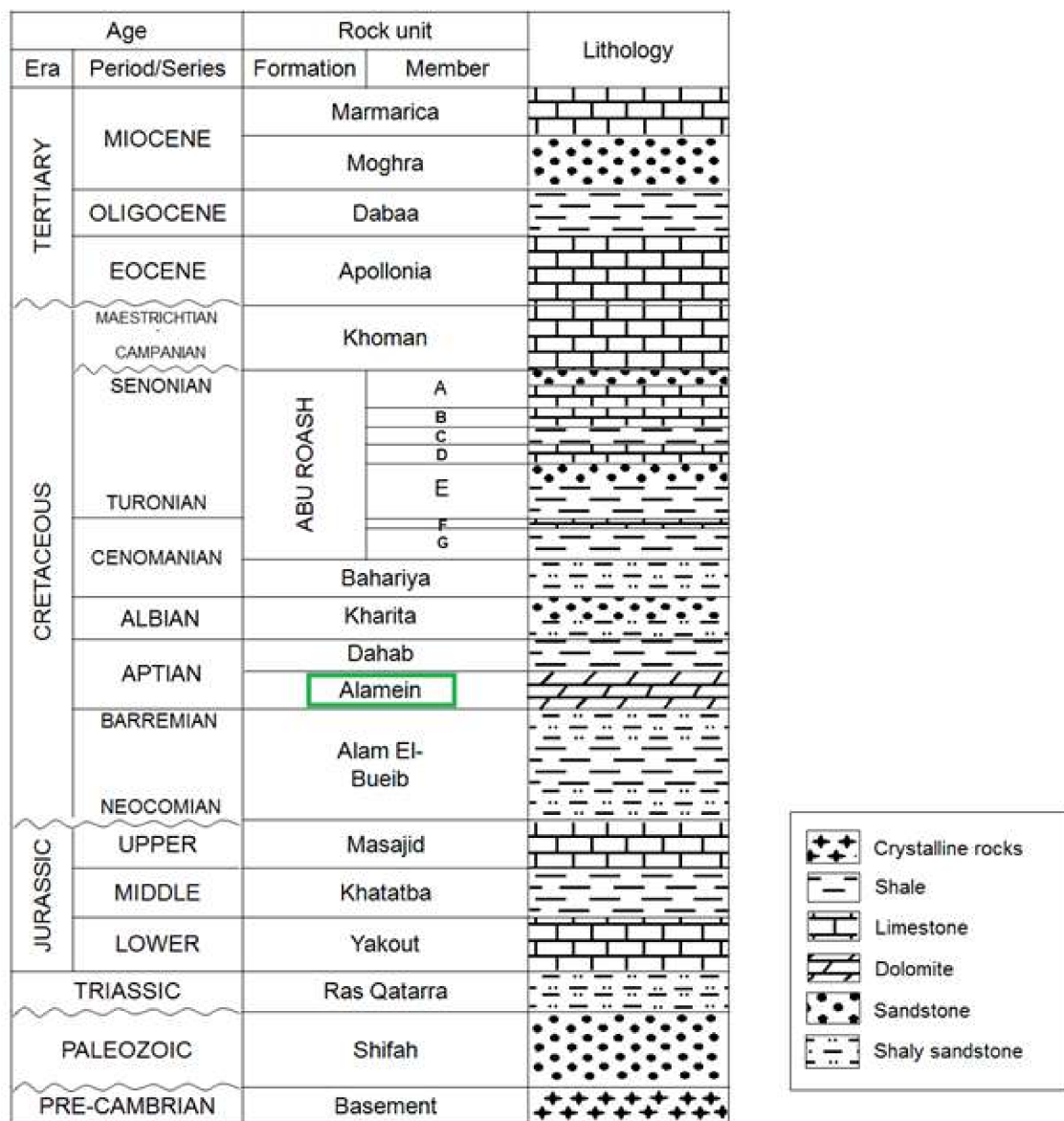
Age		Rock unit		Lithology
Era	Period/Series	Formation	Member	

Figure 2. Litho-stratigraphic column of the north Western Desert of Egypt, modified version of [31].

3. Materials and Methods

3.1. Well Logging and Petrophysical Data

For the present study, wireline log data two vertical wells, Tourmaline-1X and N.Alamein-6X, were used.Tourmaline-1X well was logged from 8880–9450 ft and N.Alamein-5X well 3656–11,655 ft. The log suite includes several conventional one-dimensional logs, including gamma ray, caliper, neutron, density, sonic and shallow and deep resistivity logs. The following logged intervals have been used for the evaluation: Tourmaline-1X 9070 to 9370 ft (total thickness of 300 ft); N.Alamein-6X 8954 to 9278 ft (total thickness of 324 ft). The upper part of the N.Alamein-6X (8954–8988.15 ft) was identified as pure shale based on the analysis of the wireline log data and was excluded from the study. Interpretation of wireline log data was performed using the Interactive Petrophysics (IP) 4.2 software package developed by LR Senergy (Scotland, UK). The neutron-density equation is used to compute porosity and the dual water equation is used to evaluate the water saturation value Additionally, density vs. neutron cross-plot has been applied for determination of the expected formation lithology.

Sonic vs. neutron-density cross-plot has also been produced to classify the type of porosity between primary and secondary. Sonic porosity is calculated based on the Wyllie Equation.

3.2. Formation MicroScanner

A Formation MicroScanner (FMS) has been used to image the Tourmaline-1X well at specific depth interval between 9070 and 9636 ft. It is a downhole resistivity imaging tool, which provides an image of the wellbore wall based on resistivity contrasts [32]. It has four orthogonal pads each containing 16 electrodes. The pads are in direct contact with the borehole wall and scan formation by 2.4 mm vertical sampling rate [33]. Each electrode independently measures resistivity of formation. The measured resistivity is then converted into an image illustrating resistivity contrast in the borehole wall [33]. On the FMS log, light shaded areas indicate high resistivity zones while dark shaded areasindicate zones with low resistivity response. After the FMS data is processed, interpretation is done to characterize geological features around the drilled borehole such as fractures, bedding planes and voids/vugs or channels.

3.3. Core Photographs under White and UV Light

Photographs of core samples under white light and ultraviolet (UV) light for the depth intervals between 9088 and 9113 ft of N.Alamein-5X well have been used for the study. Long-wave ultraviolet (UV) causes most hydrocarbons to fluoresce in the visible green, blue or red spectra ranges [34,35]. Although fluorescence under UV itself is insufficient to verify the presence of mobile oil due to the probable presence other sources of fluorescence (e.g., fluorescent minerals, OBM/lubricants used, dead oil or bitumen and gilsonite cement), it could still help to prove the presence of considerable total hydrocarbon-enriched secondary porosity in the carbonate reservoir. In the situation of known low primary porosity, this observation can be an indication of the presence of secondary porosity structures.

4. Results

4.1. Interpreted Well Logs and Petrophysical Results

Available conventional one-dimensional subsurface wireline log data from two wells in the study area, the Tourmaline-1X well (Figure 3) and the N.Alamein-6X well (Figure 4), show that the Alamein Formation is predominantly a dolomitic layer with abundant secondary porosity. Average petrophysical properties for both wells (see Table 1) indicate good reservoir quality of Alamein Formation. Interpretation of well data for the N.Alamein-6X well is similar to the first well and yields similar results (see Figures 4 and 5). Neutron–density porosity vs. sonic porosity cross-plots using the Wyllie Equation (Figure 6) shows that the porosity in the Alamein dolomite formation is highly influenced by secondary porosity.

Table 1. Petrophysical parameters for Alamein Formation for Tourmaline-1X and N.Alamein-6X wells.

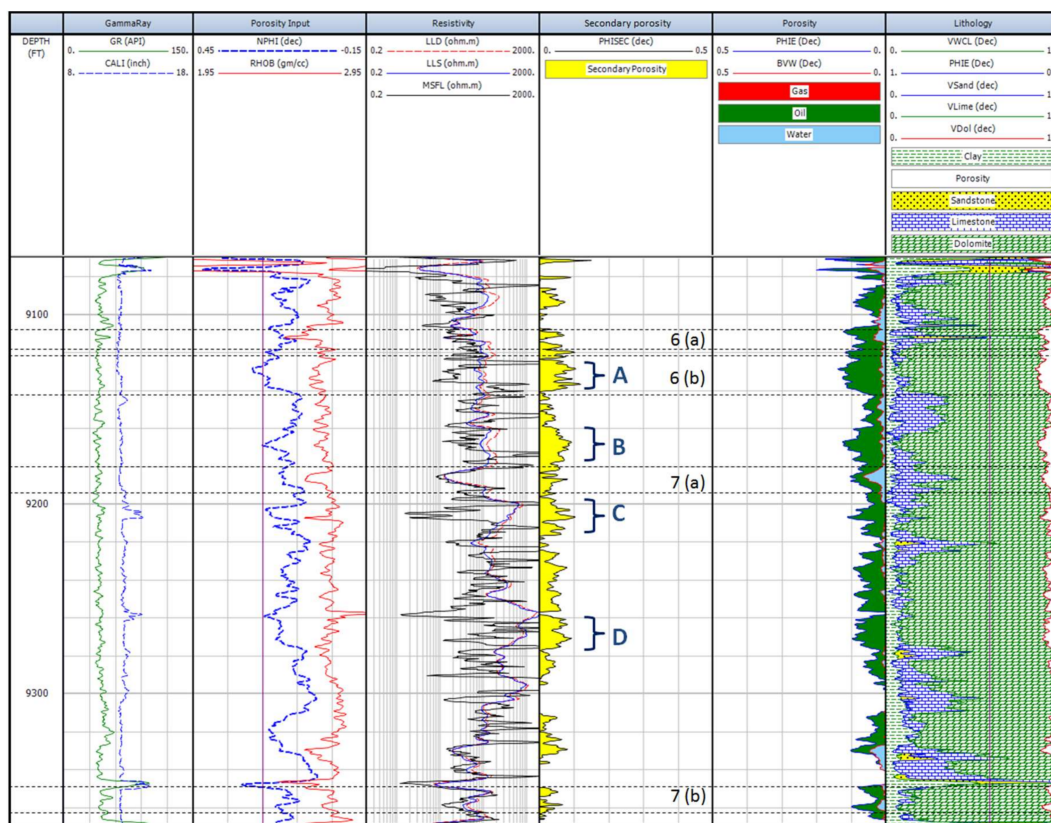| Borehole Wells | Top (ft) | Thickness/Net | | | | Porosity | | Fluids | |
		Bottom (ft)	Gross (ft)	Net Reservoir (ft)	Net Pay (ft)	Ave PHIE (%)	V_{sh} (%)	Ave S_w (%)	Ave S_h (%)
Tourmaline-1X	9070	9370	300	172.8	158.8	8	6.2	24.6	75.4
N.Alamein-6X	8988.5	9278	289.5	64.6	63.9	11.4	4.7	27.4	72.6

Figure 3. Analysis of well logging data for Tourmaline-1X showing high secondary porosity in the Alamein Formation, where zones with greatest secondary porosity are labeled (**A**–**D**), and 6(**a**)–6(**b**) and 7(**a**)–7(**b**) are intervals where image log is utilized.

4.2. Secondary Porosity Derived from FMS

Evaluated Alamein Formation is considerably affected by diagenesis, which resulted in the creation of several types of secondary porosity structures. The major secondary porosity features identified in Tourmaline-1X well are (A) vugs, (B) drilling-induced factures and (C) channels.

(A)   Vugs

In the Tourmaline-1X well, FMS indicates that vuggy pores are very abundant and dominant across the whole studied interval (Figures 7 and 8). These vugs vary in size and exist in forms of isolated and interconnected vugs. For example, a majority of isolated vugs is located in the interval of 9113.7–9118.4 ft (see Figure 7a). However, considering the two-dimensional nature of the FMS image, this assumed poorly-connected pore may well be connected. A large vug network is located in the interval between 9106 and 9111 ft. A number of poorly-interconnected smaller vugs also exist in intervals 9180–9182.5 ft and 9189–9191 ft. Besides these observations, however, most of the vugs in the studied Alamein Formation are well-connected. This fact correlates with the results of the petrophysical interpretation which yields high effective porosity values (Table 1). For example, vugs of various sizes are located in the zone 9121 ft–9139 ft (Figure 7b). Good quality carbonate reservoir sections containing abundant secondary porosity structures are observed at 9182.5–9189 ft and between 9357 ft and 9362 ft (Figure 8b). These vuggy intervals are in parallel agreement with the secondary porosity information obtained from well logs (Figures 3 and 4), indicating good agreement between the two methods.

(B)   Fractures

Drilling-induced vertical fractures can be seen in Tourmaline-1X well at the interval between 9113 ft and 9119 ft (Figure 7a) and are almost parallel to the borehole.

(C)   Channels

The Alamein Formation in the Tourmaline-1X well has numerous dissolution channels (Figures 7b and 8b).
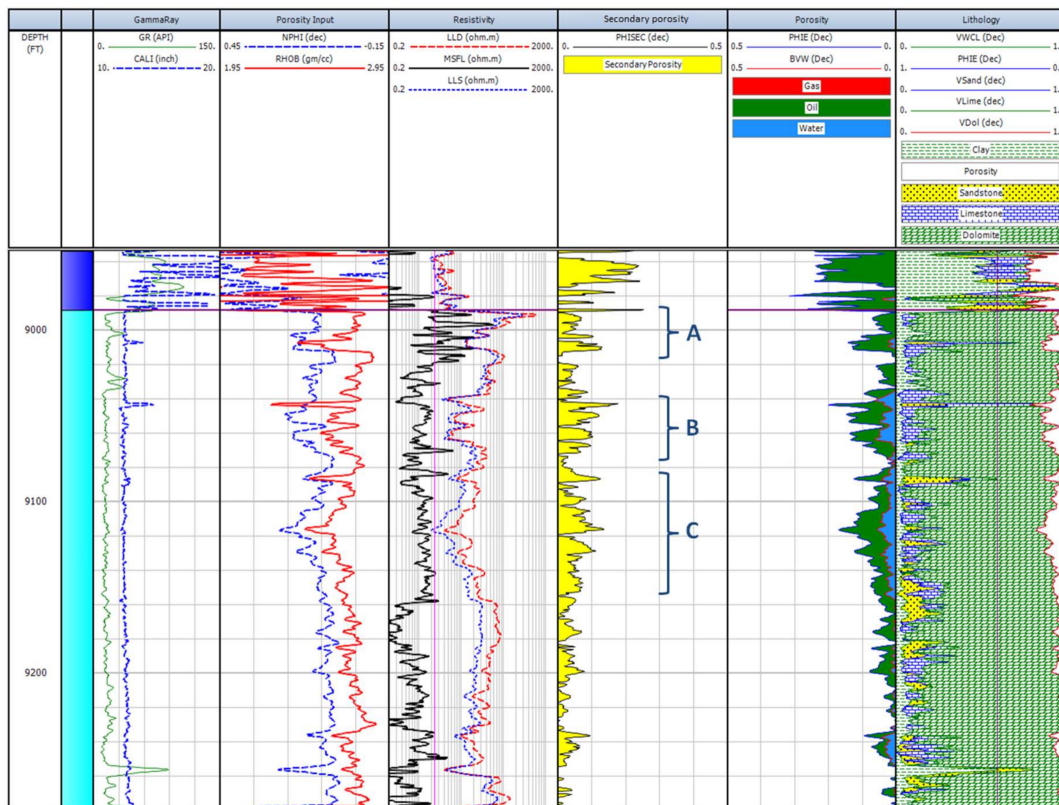

Figure 4. Analysis of well logging data for N.Alamein-6X showing high secondary porosity in the Alamein Formation, where zones with greatest secondary porosity are labeled A–C. Secondary porosity, fluid composition and lithology were derived using the same approach as described in the subscription for Figure 3.

4.3. Core Evaluation Using White Light and UV Light

The Alamein Formation core samples from the N.Alamein-5X well exhibit bright yellow fluoresce upon exposure to UV light (Figure 9). Intensive fluorescence is observed at depths of 9101, 9107 and 9111 ft (Figure 9a–c), respectively. Some areas exhibit dark blue hues, most notably 9088, 9094 and 9095 ft (Figures 8a and 9a,b), respectively.
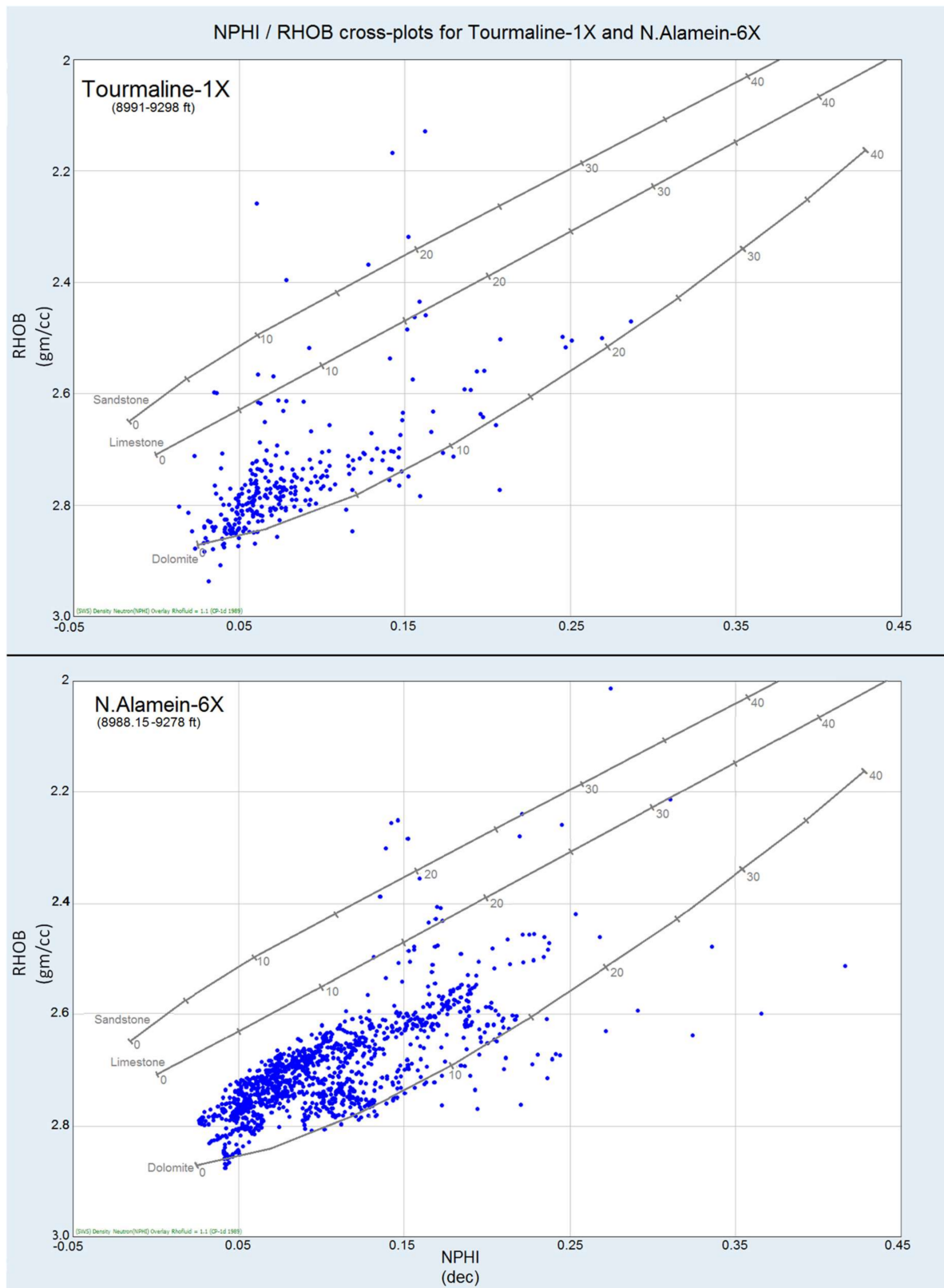
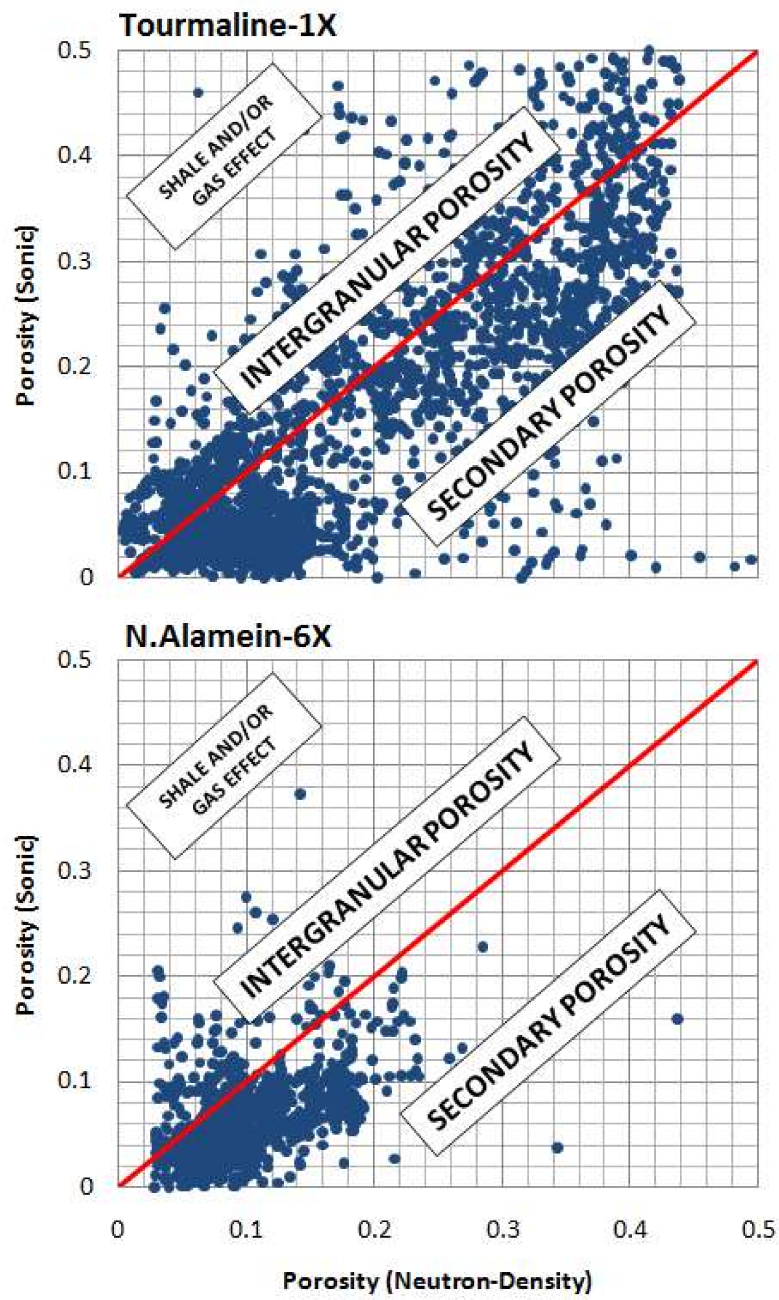**Figure 5.** Neutron (NPHI)–Density (RHOB) lithology cross-plots for Tourmaline-1X and N.Alamein-6X wells.

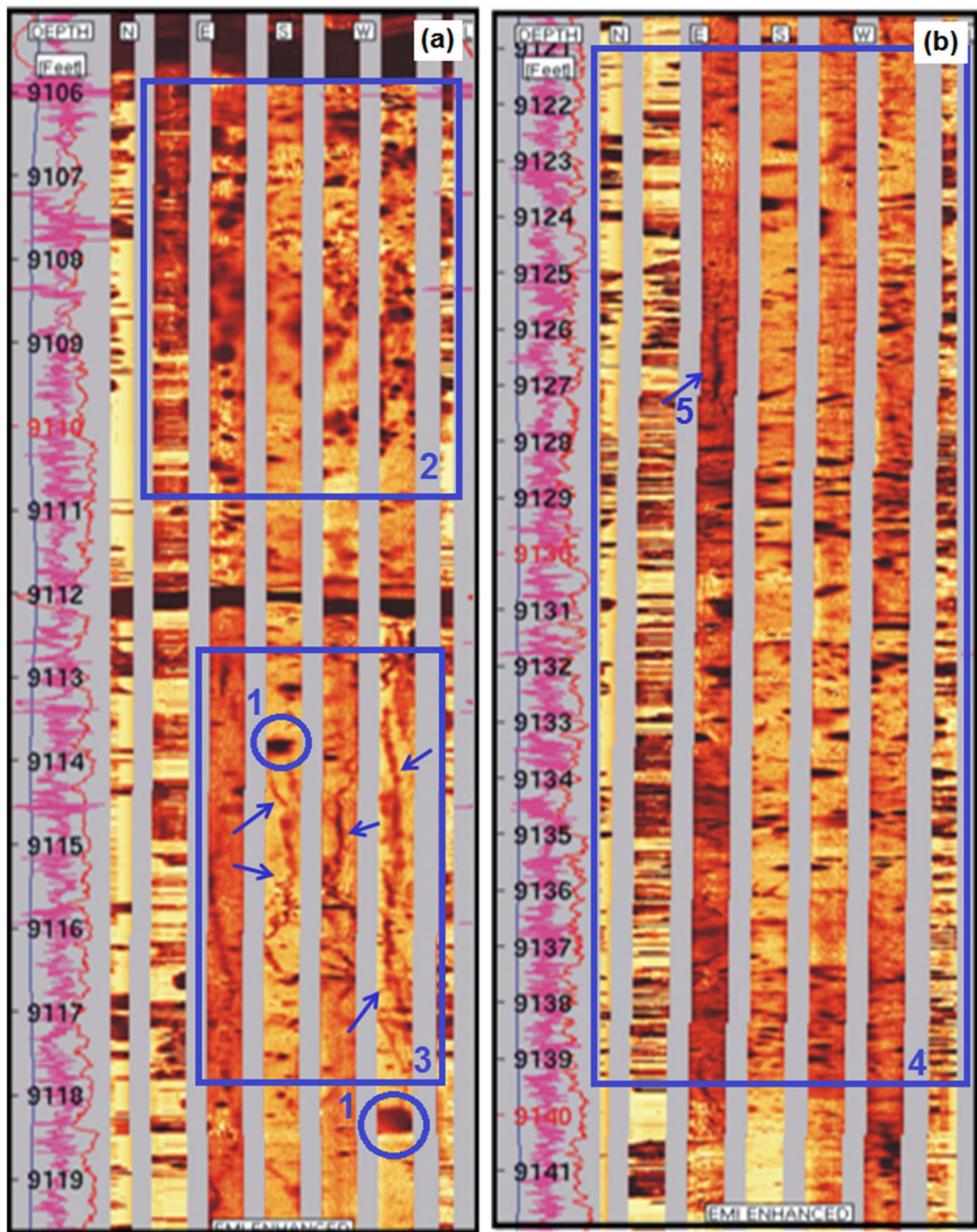**Figure 6.** Neutron–density vs. sonic porosity cross-plots for porosity evaluation.

Figure 7. FMS log showing secondary porosity structures observed in Tourmaline 1-X well
(**a**) 9106–9119 ft and (**b**) 9121–9141 ft. 1: Large isolated vugs at 9113.7–9118.4 ft; 2: Large vug network at
9106–9111 ft; 3: Drilling-induced fractures (indicated by the arrows) at 9113–9119 ft; 4: vugs of various
sizes at 9121–9129 ft; 5: Dissolution channel (indicated by the arrow).
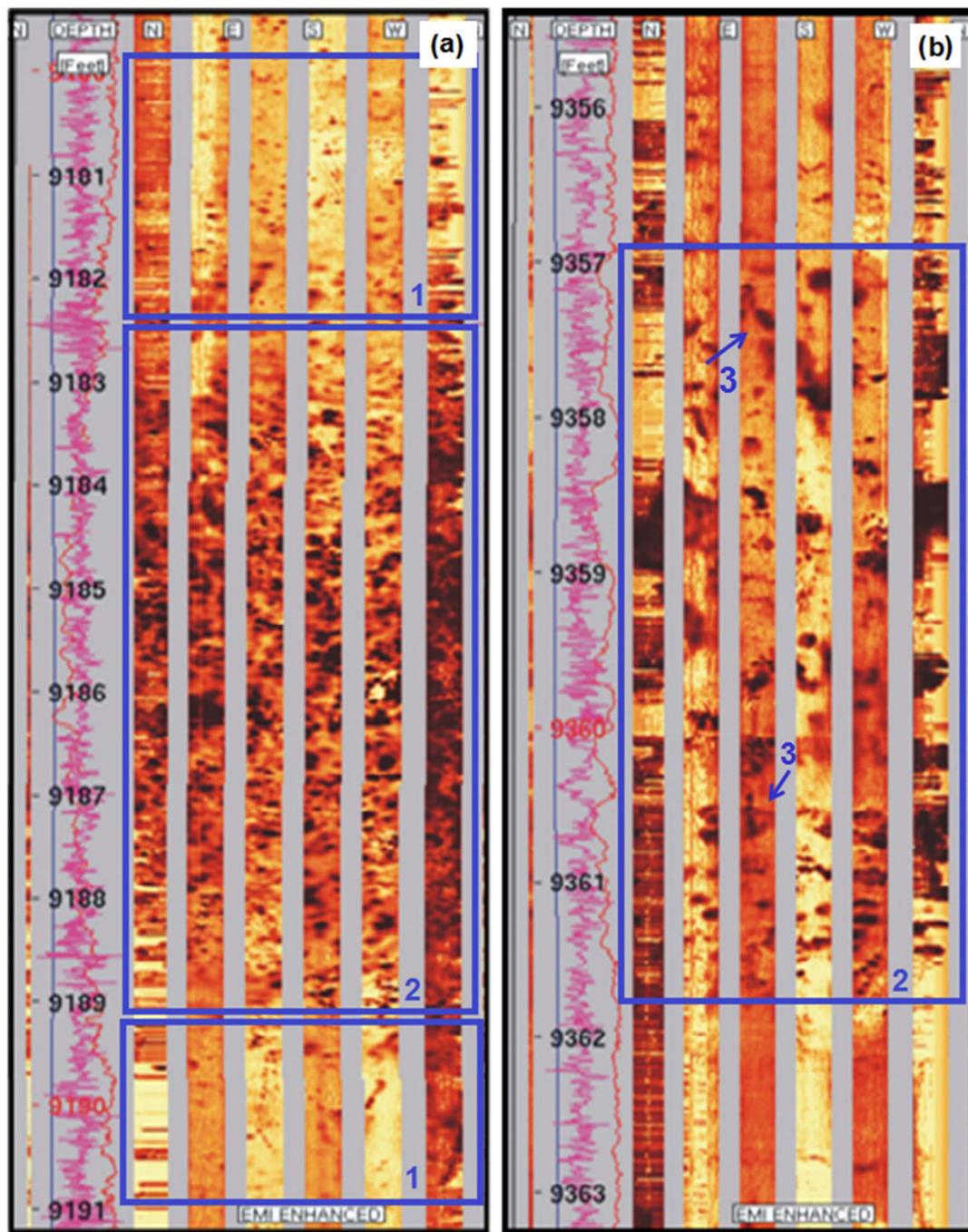
Figure 8. FMS log showing secondary porosity structures observed in Tourmaline-1X well (**a**) 9180–9191 ft and (**b**) 9356–9363 ft. 1: Many small poorly-interconnected vugs at 9180–9182.5 ft and 9189–9191 ft; 2: Multiple interconnected vugs at 9182.5–9189 ft and 9357–9362 ft 3: Dissolution channels (indicated by the arrows).
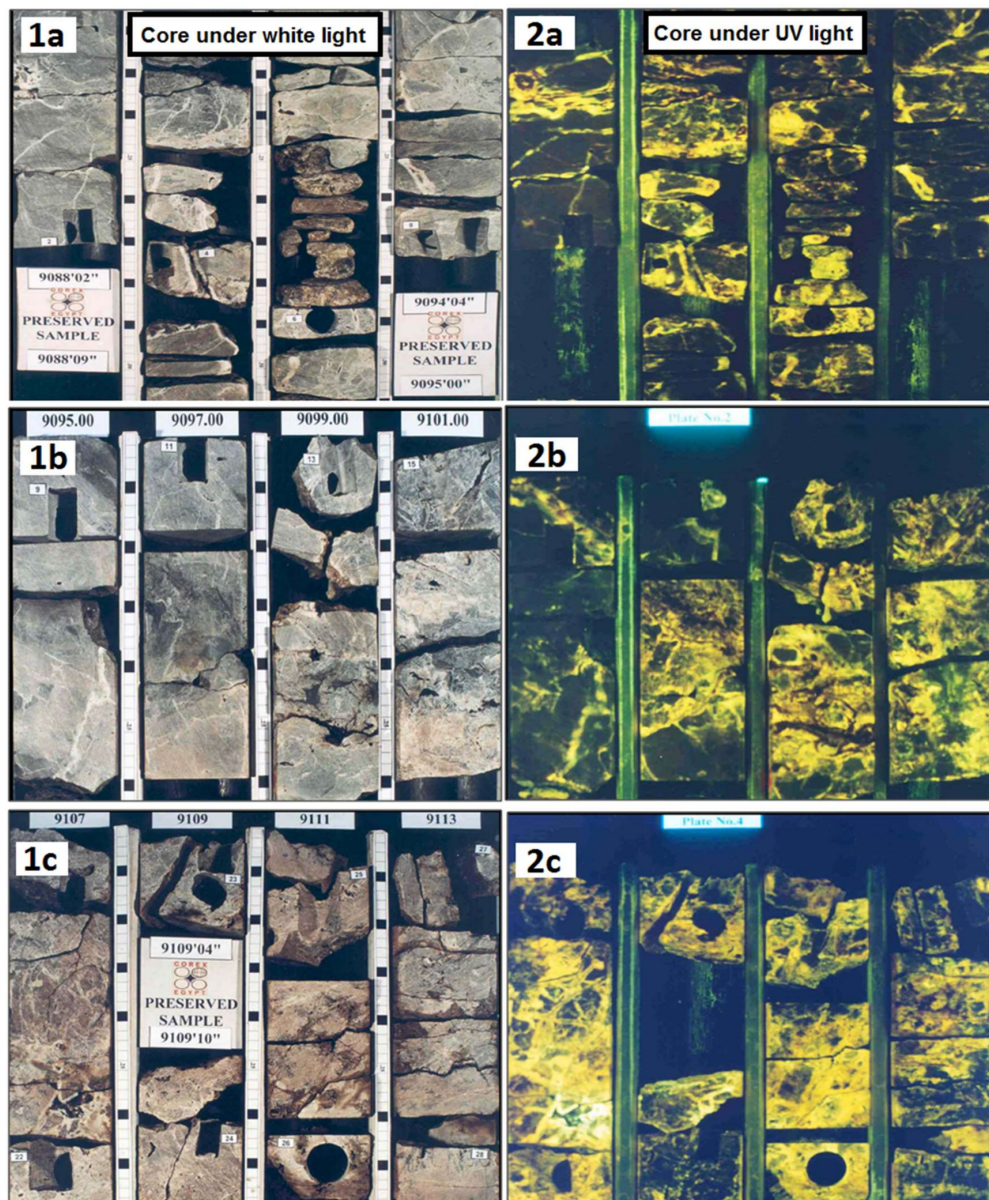
Figure 9. Photographs of core samples from the N.Alamein-5X well under white (**1a**–**1c**) and ultra violet (**2a**–**2c**) light.

5. Discussion

5.1. Interpreted Well Logs and Petrophysical Results

For the Tourmaline-1X well, the gamma ray log shows low shale content. The gamma ray log detects naturally occurring gamma radiation, and, in particular, shales usually emit more gamma rays than other sedimentary rocks. The combination of neutron and density logs provides a good source of porosity data. The positive separation observed on the neutron–density log overlay is positive for dolomite, with limestone or calcite intervals observed at several depths. This observation is in agreement with the NPHI-RHOB cross-plot (Figure 5), which shows that the studied formation is primarily formed of dolomite and calcareous dolomite. Neutron and density porosity logs are used in this study to infer lithology and fluid content (refer to Section 3.1). Deep lateralog (LLD) measures the true formation resistivity, whereas micro-spherical focused log (MSFL) evaluates the borehole resistivity. Due to its poor conductivity nature, where hydrocarbon is present, the resistivity values are

high. Thus, large separation between MSFL and LLD resistivities (Figure 3) indicates oil bearing zones. Both secondary porosity and effective porosities, derived from the wireline log data, remain significant across the pay. The zones with the highest secondary porosity (annotated A–D in Figure 3) are located in hydrocarbon-bearing intervals of 9124–9130 ft, 9160–9178 ft, 9198–9216 ft and 9260–9268 ft. Based on the results of the performed analysis the average effective porosity across the pay is estimated as 8%, and a corresponding average hydrocarbon saturation of 75.4%.

Secondary porosity for the N.Alamein-6X well is higher compared to Tourmaline-1X with zones of the highest level of the secondary porosity located in oil bearing intervals 8988–9016 ft, 9041–9072 ft and 9080–9278 ft. Defined average effective porosity is 11.4%, which is higher than for the first well with a corresponding hydrocarbon saturation of 72.6%.

The neutron–density crossplot indicating that the porosity in the Alamein dolomite formation is strongly influenced by secondary porosity supports with previous findings made by Kassab et al. [34], whose petrographical study showed that the diagenesis-influenced porosity of the Cretaceous rock samples in the study area, which included the Alamein Formation, comprises not only interparticle, but also vugs and molds, in addition to fractures and channel porosities.

5.2. Secondary Porosity Derived from FMS

FMS images are useful in this study, as they provide information regarding secondary porosity that could not be obtained from intepretation of wireline log. While logging tools could estimate the volume of secondary porosity, they could not differentiate the types, shapes and sizes of secondary pores that may be present in the studied interval. As aforementioned in the Results section, there are three main types of secondary porosity observed in the four sections assessed in the FMS images of the Tourmaline-1X well. Via borehole images, these structures are identified and differentiated accordingly.

Secondary porosity, which is observed in abundance in the Alamein Formation, is a product of diagenesis. Diagenesis involves the mineralogical and textural changes undergone by a rock when they are brought into contact with waters of varying chemical composition. Secondary porosity is produced by the diagenetic process of dissolution, whereby carbonate minerals are dissolved and removed, thus creating and modifying pore space in reservoir rocks. The effect of this process on permeability depends upon the geometry and location of the resulting voids relative to the rock fabric. Secondary dissolution may be fabric-selective and results in formation of isolated pores, or it may enlarge fractures and interparticle pores resulting in large, connected pores. The types of secondary porosities encountered include: moldic, channel, inter-crystalline, fracture or vuggy porosity. In this study, vugs and channels were observed. A majority of the vugs in the studied Alamein Formation are well-connected, which support the secondary porosity information intepreted from well logs (Figures 3 and 4), indicating good integration between the two methods.

Drilling-induced fractures (DIF), on the other hand, are a product of drilling. DIFs are dependent on the rock properties. When the drilling pressure exceeds the elasticity limit of the rock, it may not be able to withstand this pressure and may fracture as a result. Carbonates are relatively highly rigid in nature, and consequently have low elasticity, which makes them more susceptible to fracture. Unlike natural fractures that tend to cross-cut the wellbore, DIFs typically develop as narrow, sharply defined features that are sub-parallel or slightly inclined to the borehole axis in vertical wells.

Overall, from the borehole image logs, we conclude that the dolomitic Alamein Formation in the evaluated interval contains abundant secondary porosity structures, including vugs, channels and fractures. Location of the zones with these structures (see Figures 7 and 8) correlates with depths of the zones having higher secondary porosity values according to the interpretation of the well logging data (see Figures 3 and 4). The interpreted secondary porosity from the FMS images in this study is in parallel agreement with the petrographic study by Kassab et al. [36], where Alamein Formation contains abundant vugs, molds, fractures and channel porosities.

5.3. Core Evaluation Using White Light and UV Light

It can be concluded that the bright yellow fluorescence is consistent with oil-bearing dolomite, magnesite and limestone rocks, which typically fluoresce with yellow, yellowish brown to dark brown color under UV light [37]. This confirms the presence of hydrocarbon-filled porosity. To some extent, the observed fluorescence reflects the degree of hydrocarbon content in each zone: the stronger it is, the higher is the hydrocarbon content.

6. Conclusions

Analysis of wireline logs for Tourmaline-1 and N.Alamein-6X wellsf or the Alamein Formation indicates the presence of secondary porosity across the evaluated depth ranges (9070–9370 ft and 8954–9278 ft correspondingly). Secondary pores are located in hydrocarbon-reach zones with hydrocarbon saturation levels of over 70%. Application of the Formation MicroScanner (FMS) image logging enabled further understanding on the types and morphological configuration of these secondary pore spaces, which could not be identified by the well logging data. FMS images of Tourmaline-1X well confirm the presence of different secondary porosity structures, which are vugs, drilling-induced fractures (DIF) and dissolution channels, across the evaluated depth intervals. The vugs are observed to be interconnected, which support the evaluation of the petrophysical data for the same well, which reveals that the average effective porosity is 8% across the pay studied interval. The presence of hydrocarbons in the zones with high secondary porosity was further confirmed by the fluorescence of core samples from the N.Alamein-5X well. This integrated study provides a further contribution to the understanding of the production performance of the Alamein Dolomite Formation.

References

1. Roehl, P.O.; Choduette, P.W. *Carbonate Petroleum Reservoirs*; Spring: New York, NY, USA, 1985; p. 622.
2. Khoshbakht, F.; Azizzadeh, M.; Memarian, H.; Nourozi, G.H.; Moallemi, S.A. Comparison of electrical image log with core in a fractured carbonate reservoir. *J. Petrol. Sci. Eng.* **2012**, *86–87*, 289–296. [CrossRef]
3. Abd El-Gawad, E.A. The use of well logs to determine the reservoir characteristics of Miocene rocks at the Bahar Northeast Field, Gulf of Suez, Egypt. *J. Petrol. Geol.* **2007**, *30*, 175–188. [CrossRef]
4. Hakimi, M.H.; Shalaby, M.R.; Abdullah, W.H. Application of well log analysis to assess the petrophysical patterns of the Lower Cretaceous Biyad Formation, East Shabowah Oilfields, Masila Basin, Yemen. *World Appl. Sci. J.* **2012**, *16*, 1227–1238.
5. Lahsin, A.; Morgen, S. Analysis of well log and pressure data of the gas-bearing sand reservoirs of Kafr El-Sheikh formation: Case study from the off-shore Nile Delta-Egypt. *Int. J. Phys. Sci.* **2012**, *7*, 5353–5366.
6. Ahmed Abdel-Rahman, A.Y. Well log analysis and hydrocarbon potential of the Khoman Formation, GPT Field, North Western Desert, Egypt. *World Appl. Sci. J.* **2013**, *28*, 2288–2301.
7. Shalaby, M.R.; Islam, M.A. Fracture detection using conventional well logging in carbonate Matulla Formation, Geisum Oilfield, Gulf of Suez, Egypt. *J. Petrol. Explor. Prod. Technol.* **2017**, *7*, 977–989. [CrossRef]
8. Jumat, N.; Shalaby, M.R.; Islam, M.A. Integrated reservoir characterization of the Paleocene Farewell Formation, Taranaki Basin, New Zealand, using petrophysical and petrographical analyses. *J. Petrol. Expl. Prod. Technol.* **2017**, 1–17. [CrossRef]
9. Swee, P.D.; Shalaby, M.R.; Islam, M.A. Integrated Reservoir Characterization Study of the McKee Formation, Onshore Taranaki Basin, New Zealand. *Geosciences* **2018**, *8*, 105.

10. Nurmi, R.; Charara, M.; Waterhouse, M.; Park, R. Heterogeneities in carbonate reservoirs: Detection and analysis using borehole electrical imagery. In *Geological Applications of Wireline Logs*; Hurst, A., Lovell, M.A., Morton, A.C., Eds.; Geological Society of London Special Publication: London, UK, 1990; Volume 48, pp. 95–111.

11. Akbar, M.; Vissapragada, B.; Alghamdi, A.H.; Allen, D.; Herron, M.; Carnegie, A.; Dutta, D.; Olesen, J.R.; Chourasiya, R.D.; Logan, D.; et al. A snapshot of carbonate reservoir evaluation. *Schlumberger Oilfield Rev.* **2000**, *12*, 20–41.

12. Russell, S.D.; Akbar, M.; Vissapragada, B.; Walkden, G.M. Rock types and permeability prediction from dipmeter and image logs: Shuaiba reservoir (Aptian), Abu Dhabi. *AAPG Bull.* **2002**, *86*, 1709–1732.

13. Ahr, W.M.; Allen, D.; Boyd, A.; Bachman, H.N.; Smithson, T.; Clerke, E.A.; Gzara, K.B.M.; Hassal, J.K.; Murty, C.R.K.; Zubari, H.; Ramamoorthy, R. Confronting the carbonate conundrum. *Schlumberger Oilfield Rev. Spring* **2005**, *17*, 18–29.

14. Wilson, M.E.; Lewis, D.; Yogi, O.; Holland, D.; Hombo, L.; Goldberg, A. Development of Papua New Guinean onshore carbonate reservoir: A comparative borehole image (FMI) and petrographic evaluation. *Mar. Petrol. Geol.* **2013**, *44*, 164–195. [CrossRef]

15. Aadnoy, B.S. Inversion technique to determine the in-situ stress field from fracturing data. *J. Petrol. Sci. Eng.* **1990**, *4*, 127–141. [CrossRef]

16. Brace, W.F. Permeability of crystalline and argillaceous rocks. *Int. J. Rock Mech. Min. Sci. Geomech.* **1980**, *17*, 241–251. [CrossRef]

17. Aydin, A. Fractures, faults, and hydrocarbon entrapment, migration and flow. *Mar. Petrol. Geol.* **2000**, *17*, 797–814. [CrossRef]

18. Gudmundsson, A. Fracture dimensions, displacements and fluid transport. *J. Struct. Geol.* **2000**, *22*, 1221–1231. [CrossRef]

19. Michie, E.A.H.; Haines, T.J.; Healy, D.; Neilson, J.E.; Timms, N.E.; Wibberley, C.A.J. Influence of carbonate facies on fault zone architecture. *J. Struct. Geol.* **2014**, *65*, 82–99. [CrossRef]

20. Michie, E.A.H. Influence of host lithofacies on fault rock variation in carbonate fault zones: A case study from the Island of Malta. *J. Struct. Geol.* **2015**, *76*, 61–79. [CrossRef]

21. Trippetta, F.; Carpenter, B.M.; Mollo, S.; Scuderi, M.M.; Scarlato, P.; Collettini, C. Physical and Transport Property Variations within Carbonate-Bearing Fault Zones: Insights from the Monte Maggio Fault (Central Italy). *Geochem. Geophys. Geosyst.* **2017**. [CrossRef]

22. Sestini, G. Egypt. In *Regional Petroleum Geology of the World, Part II: Africa, America, Australia and Antartica*; Kulke, H., Ed.; Gebrüder Borntraeger: Berlin/Stuttgart, Germany, 1995; pp. 57–87.

23. Elzarka, M.H. Mode of hydrocarbon generation and prospects of the northern part of the Western Desert, Egypt. *J. Afr. Earth Sci.* **1983**, *14*, 294–318. [CrossRef]

24. Zein El-Din, M.Y.; Matbouly, S.I.; Moussa, S.M.; Kralik, M.A. Geochemistry and oil-oil correlations in the Western Desert; Abstract. In Proceedings of the 10th Egyptian Petroleum Conference, Cairo, Egypt, 7–19 November 1990.

25. Abu el Naga, M. Paleozoic and Mesozoic depocentres and hydrocarbon generating areas, Northern Western Desert. In *Proceedings of the EGPC 7th Exploration and Production Conference*; EGPC: Cairo, Egypt, 1984; pp. 269–287.

26. Metwalli, M.H.; Abd El-Hady, Y.E. Petrographic characteristics of oil-bearing rocks in Alamein oil field: Significance of source reservoir relations in North Western Desert, Egypt. *AAPG Bull.* **1975**, *59*, 510–523.

27. Said, R. *The Geology of Egypt*; AA Balkerma: Rotterdam, The Netherlands, 1990; p. 734.

28. Ahmed, M.A. Geodynamic Evolution and Petroleum System of Abu Gharadig Basin, North Western Desert, Egypt. Ph.D. Thesis, Institute of Geology and Geochemistry of Petroleum and Coal (LEK), RWTH-Aachen University Germany, Aachen, Germany, 2008; p. 255.

29. Egypt Oil & Gas. *Egypt Production Report*; Egypt Oil & Gas: Cairo Governorate, Egypt, 2012; p. 143.

30. Badr, A.R.; Ayoub, M.R. Study of a complex carbonate reservoir using the Formation MicroScanner (FMS) Tool. In Proceedings of the SPE Middle East Oil Technical Conference and Exhibition, Manama, Bahrain, 25–28 September 1989; pp. 507–516.

31. Abdou, A. Deep wells in Khalda West: A brief review. In Proceedings of the 14th EGPC Petroleum Conference, Cairo, Egypt, 12–15 October 1998; pp. 517–533.

32. Ekstrom, M.P.; Dahan, C.; Chen, M.Y.; Lloyd, P.; Rossi, D.J. Formation imaging with microelectrical scanning arrays. In Proceedings of the SPWLA 27th Annual Logging Symposium, London, UK, 29 June–2 July 1987; Volume 28, pp. 294–306.

33. Serra, O. *Formation Micoscanner Image Interpretation*; Schlumberger Educational Service: Houston, TX, USA, 1989; p. 177.

34. Beckman, H. *Geological Prospecting of Petroleum*; Halted Press: New York, NY, USA, 1918; pp. 97–111.

35. Bowers, R.J. Rotary drilling investigative techniques and tools. In *Hydrocarbon Contaminated Soils, Volume III*; Kostecki, P.T., Calabrese, E.J., Eds.; Lewis Publishers: Chelsea, MI, USA, 1993; pp. 89–105.

36. Kasaab, M.A.; Abdou, A.A.; El Gendy, M.G.; Shehata, M.G.; Abuhagaza, A.A. Mutual relations between petrographical and petrophysical properties of Cretaceous rock samples for some wells in the North Western Desert, Egypt. *Egypt. J. Petrol.* **2013**, *22*, 73–90. [CrossRef]

37. Exploration Logging, Inc. *Mud Logging: Principles and Interpretations*; IHRDC: Boston, MA, USA, 1985; p. 92.